Nanoscale

COMMUNICATION

Check for updates

Incorporating zeolitic-imidazolate framework-8 nanoparticles into kidney scaffolds: a first step towards innovative renal therapies†

Fátima Guerrero,*[a,b] Victoria Pulido,[a,b] Said Hamad, [ID][e] Pedro Aljama,[a,b] Alejandro Martín-Malo[a,b,c,d] and Carolina Carrillo-Carrión [ID] *[f,g]

We demonstrate for the first time the potential of zeolitic-imidazolate framework-8 nanoparticles to be incorporated within a renal scaffold while retaining their ability to remove uremic toxins (mainly hydrophobic toxins like *p*-cresol) under flow conditions. This work may pave the way for the future development of novel adsorbents for dialysis and/or artificial kidneys.

[a]Maimonides Biomedical Research Institute of Cordoba (IMIBIC), Reina Sofia University Hospital, 14004 Córdoba, Spain. E-mail: fatima.guerrero@imibic.org
[b]Department of Medicine, University of Cordoba, 14004 Córdoba, Spain
[c]Nephrology Unit, Reina Sofia University Hospital, 14004 Córdoba, Spain
[d]Spanish Renal Research Network, Institute of Health Carlos III, 28040 Madrid, Spain
[e]Department of Physical, Chemical and Natural Systems, University Pablo de Olavide, 41013 Seville, Spain
[f]Institute for Chemical Research (IIQ), CSIC-University of Seville, 41092 Sevilla, Spain. E-mail: carolina.carrillo@csic.es
[g]Department of Organic Chemistry, Faculty of Chemistry, University of Seville, 41012 Seville, Spain
†Electronic supplementary information (ESI) available. See DOI: https://doi.org/10.1039/d2nr04246k

Carolina Carrillo-Carrión

Carolina Carrillo-Carrión is currently a Tenured Scientist at the Institute for Chemical Research (IIQ, CSIC-University of Seville). She received her Ph.D. from the University of Córdoba (2011). Then she worked at different universities and research centres: Philipps-Universität Marburg (Germany, as a Humboldt), CICbiomaGUNE (San Sebastián, as a JdC-I researcher), CiQUS-University Santiago de Compostela (as a Marie Curie fellow), University of Córdoba (PI of a national project for young researchers), and University of Seville (as a Ramón y Cajal researcher). Nowadays, her research is focused on developing multifunctional metal–organic frameworks for applications in the biomedical and (bio)catalytic fields.

Introduction

Chronic kidney disease (CKD), a condition characterized by a gradual loss of kidney function over time, is currently a major health problem worldwide affecting approximately 14% of the general population.[1] This syndrome leads to the accumulation in the blood of uremic toxins regularly eliminated by healthy kidneys, with the consequent appearance of toxic symptoms, persistent inflammation, oxidative stress and endothelial dysfunction, which eventually lead to major clinical complications including cardiovascular disease (CVD) and deaths.[2]

Uremic toxins are a non-traditional risk factor for CVD in CKD patients. At present, the strategy to remove or eliminate uremic toxins from the blood is by dialysis. However, some toxins cannot be effectively removed with conventional hemodialysis techniques due to their hydrophobicity and their high binding affinity to plasma proteins.[3] To overcome this limitation, much effort has been focused on developing a wide variety of membranes (with different cut-offs, low/high-flux, and modified composition),[3,4] as well as on investigating alternative dialysis techniques such as post-dilution on-line hemodiafiltration[5] or expanded hemodialysis.[6] Currently, adsorption-based techniques seem to be the most effective strategy to improve the toxins removal. Among the literature reports on the use of materials such as zeolites,[7,8] ordered mesoporous carbons,[9] and metal–organic frameworks (MOFs),[10–14] the latter are still underexploited, most likely due to biocompatibility issues. On the other hand, many of these adsorbent materials lack enough efficiency and/or selectivity, which leads to the removal of useful molecules and massive amounts of albumins that can ultimately cause serious complications such as hypoalbuminemia. Therefore, the development of alternative dialytic materials that have combined advantages

of high efficiency, good selectivity towards certain toxins, and adequate biocompatibility still remains a challenge.

MOFs, which are a class of porous materials constructed using metal-containing units (secondary building units) and organic linkers,[15] have attracted much interest in adsorption applications due to their structural and functional tunability and porosity (e.g., hydrophilic/hydrophobic nature, adjustable pore size, and incorporation of chemical groups for selective interactions). Within the context of CKD, recent works have examined the adsorption of uremic toxins onto several MOF types to design high-capacity MOF-based adsorbents, with the ultimate goal of implementing dialysis systems. Kato et al. reported that NU-1000, a zirconium-based MOF, efficiently extracted two uremic toxins, namely potassium p-cresyl sulfate (pCS) and potassium indoxyl sulfate (IS), free in aqueous media and when bound to human serum albumin (HSA) proteins.[11] By isothermal titration calorimetry, they concluded that those toxin–MOF interactions were both enthalpically and entropically driven.[12] More recently, Cuchiaro et al. demonstrated that an iron-based MOF, i.e. MIL-100(Fe), had a greater adsorption efficiency for pCS than the previously reported Zr-based MOFs.[13] This adsorption enhancement was attributed to the direct coordination through electrostatic interactions of pCS with vacant metal sites in the MOF, besides the interactions occurring at the organic linker sites. Another Zr-based MOF, specifically UiO-66, was also tested for removing several toxins from an aqueous solution,[11,14] and importantly, it was found that both the presence of structural defects within the framework and the incorporation of $-NH_2$ groups increased the adsorption capacity of UiO-66 in comparison to the pristine defect-free UiO-66.[14] Despite the promising results reported to date, the performance of MOFs as potential adsorbents for uremic toxins was assessed under "idealized conditions", i.e. experiments performed using an aqueous solution of target toxins, which are quite far from a realistic scenario in clinical practice. Furthermore, these mentioned works have focused mainly on removing toxins in their hydrophilic form (i.e., sulfate derivatives), whereas the fraction of free p-cresol (pC, in its native unconjugated form), even being found in a much smaller fraction in the serum of CKD patients, seems to have a more negative impact on the progression of CKD. For example, it was found that pC exhibited higher potency than pCS to stimulate low-density lipoprotein uptake by activating macropinocytosis,[16] which might have contributed to increased cardiovascular risk in patients with CKD. pC was also found to disrupt the endothelial progenitor cell function while its sulphonated derivative pCS does not.[17] These findings indicate that this minority fraction of free pC in CKD patients should not be overlooked.

Surprisingly, zeolitic imidazolate frameworks (ZIFs), built with tetrahedral metal ions (Zn^{+2} in the case of ZIF-8) and imidazolate linkers, have not been still investigated for the elimination of uremic toxins, even if they are one of the most used MOFs in the biomedical field because of their good biocompatibility and minimal cytotoxicity. This is probably because of the limited stability of the nano-sized ZIF-8 particles in

aqueous media and some buffers;[18] however, the coating of ZIF-8 particles with polymers has already been demonstrated to be an easy and effective approach to overcome this limitation.[19,20]

With these challenges in mind, herein we report the potential of a polymer-functionalized ZIF-8 nanoparticle (nanoZIF8@PMA) to be immobilized in a renal scaffold and restore its functionality to remove uremic toxins under flow perfusion (Scheme 1). In principle, nanoZIF8@PMA combines a number of unique features that make it an ideal nanomaterial for this application, such as (i) optimal particle size and surface chemistry, to allow physicochemical interactions with the extracellular matrix (ECM) and thus be retained in the scaffold; (ii) hydrophobic nature of its pores together with its high internal surface area, to enable effective and efficient binding of hydrophobic uremic toxins; (iii) hydrophilic nature of the surface coating, to confer biocompatibility; and (iv) minimal cytotoxicity due to the intrinsic composition of the framework (zinc ions and methylimidazole ligands).

Results and discussion

nanoZIF8@PMA particles were prepared in two steps: nano-sized ZIF-8 particles were first synthesized, followed by a post-synthetic surface functionalization procedure to incorporate the polymer that endowed the particles with a hydrophilic surface coating to provide colloidal stability in aqueous media and promote interactions with the renal scaffold. Briefly, ZIF-8 nanoparticles (nanoZIF8) were synthesized in an aqueous solution at room temperature (RT ~22 °C), using $Zn(NO_3)_2$ and methylimidazole (MeImz) as the Zn^{2+} source and organic linker, respectively, and hexadecyltrimethylammonium bromide (CTAB) was added during the synthesis which acted as a shape- and size-controlling agent.[19] The synthesis conditions (ratio of precursors, CTAB concentration, and growth time; see the ESI† for details) were optimized to obtain highly homogeneous particles with an average size of ~120 nm and a
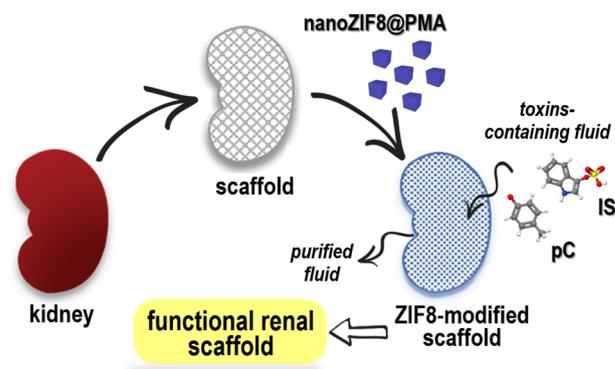
Scheme 1 Schematic illustration of the use of nanoZIF-8@PMA to modify a renal scaffold and provide it with the necessary functionality to eliminate uremic toxins, specifically p-cresol (pC) and indoxyl sulphate (IS).

cubic shape (Fig. S1†). These as-obtained nanoZIF8 particles exhibited the characteristic Bragg peaks of ZIF-8, as shown by powder X-ray diffraction (PXRD) (Fig. S2†). Next, they were post-functionalized with an amphiphilic polymer (PMA; (poly [isobutylene-*alt*-maleic anhydride]-*graft*-dodecyl) following a previously reported protocol.[19,20] After this polymer modification, the average size of the particles did not change, but the corners of the original square nanoparticles became slightly rounded, as determined by scanning electron microscopy (SEM, Fig. 1A, B and S1†). No effect on the crystalline nature of ZIF-8 after polymer functionalization was observed (Fig. 1C and S2†); notably, these PMA-modified ZIF-8 particles (in the following referred to as nanoZIF8@PMA) retained their crystalline sodalite structure after 24 h of incubation with phosphate buffered saline (PBS, 0.1 M, pH 7.4) and with solutions of toxins (0.5 mM pC or IS in PBS) as determined by PXRD, whereas pristine nanoZIF8 lost its crystallinity when exposed to PBS (Fig. 1A and S2†). This latter observation is due to the competition of the phosphate species for the Lewis metal centers (Zn^{2+} ions), releasing progressively MeImz in solution and leading to the formation of insoluble inorganic by-products as previously reported.[18] Besides, PMA functionalization endowed the particles with colloidal stability in PBS and importantly also in the presence of uremic toxins (pC and IS at 0.5 mM) as confirmed by dynamic light scattering (DLS, Fig. 1D and Table S1†). Additionally, ^{1}H Nuclear Magnetic

Resonance (^{1}H NMR) was carried out to confirm again the successful modification of nanoZIF8 particles with PMA (Fig. S3†), and thermogravimetric analysis (TGA) allowed us to determine that the amount of polymer in the nanoZIF8@PMA particles was 36 wt% (Fig. S4†). Regarding the textural properties, although the isotherms showed in principle a decrease in the surface area after PMA modification (Fig. S5†), the actual specific surface area (S_{BET}) and micropore volume (V_{micro}) of nanoZIF8@PMA were almost identical after correction considering exclusively the ZIF-8 weight (Table S2†). On the other hand, the pores of these nanoZIF8@PMA particles remained accessible to the adsorption of molecules, as demonstrated in a previous work[20] and confirmed also in this work upon exposure to uremic toxins.

Finally, it is worth noting that this synthetic approach for preparing nanoZIF8@PMA is facile, cheap, green, and easily scalable, which are important aspects in view of a future potential translation to clinics.

First, the adsorption efficiency of two common uremic toxins (pC and IS) was examined on the as-synthesized nanoZIF8@PMA by incubation of these nanoparticles with toxin solutions under static conditions, and the amount of toxins adsorbed was quantified indirectly by UV-Vis spectroscopy by measuring the toxins remaining in the supernatants after centrifugation of the particles (Fig. S6†). pC and IS concentrations were set at 0.3 mM in all experiments, trying
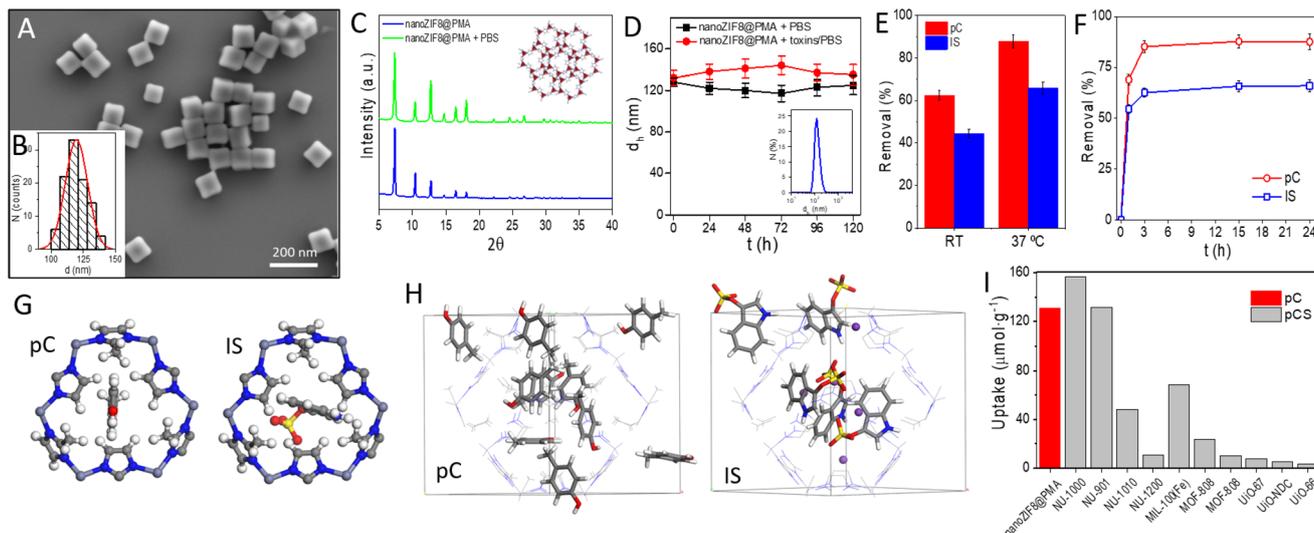

Fig. 1 (A) Representative SEM micrograph of the nanoZIF8@PMA particles. (B) Histogram of the number distribution N of the diameter d of the nanoZIF8@PMA particles (idealized as spherical particles) as determined from the SEM micrographs, d = (120 ± 9) nm. (C) PXRD pattern of the nanoZIF8@PMA particles freshly prepared and after 24 h of incubation with PBS (100 mM, pH 7.4). Inset: Crystal structure of ZIF-8 with the sodalite framework topology and showing the ordered porous network. The six-ring pore aperture has a diameter of 3.4 Å. Color code: ZnN_4 = red tetrahedra; N = blue, C = grey, and H = white. (D) Colloidal stability over time of the nanoZIF8@PMA particles dispersed in PBS or a toxin solution, as determined by DLS. Inset: DLS size distribution by the number of particles dispersed in PBS. (E) Removal efficiency of nanoZIF8@PMA (10 mg) towards pC and IS (0.3 mM in PBS) after 24 h of incubation as a function of the incubation temperature. (F) Kinetic adsorption studies at 37 °C of nanoZIF8@PMA (10 mg) towards pC and IS (0.3 mM in PBS). (G) View of a 6-membered ring window of the ZIF-8 structure, through which pC and IS molecules must pass to diffuse within the framework. Colour code: H = white; C = grey; N = blue; O = red; and S = yellow. (H) View of the ZIF-8 structure in which pC or IS molecules have been adsorbed, using GCMC simulations. Colour code: H = white; C = grey; N = blue; O = red; S = yellow; and K = violet. The H atoms of the framework structure have been omitted for clarity. (I) Comparative uptake between the MOFs synthesized in this work (nanoZIF8@PMA) and those reported by Kato *et al.*[11] and Cuchicharo *et al.*[13] using different MOFs. pC = *p*-cresol and pCS = *p*-cresyl sulfate.

to simulate the blood of CKD patients.[3] Different conditions were studied, specifically, the amount of nanoZIF8@PMA particles and the time and temperature of incubation. First, various amounts of nanoZIF8@PMA particles (5 mg, 10 mg, 15 mg, and 20 mg) were added to each solution of pC and IS, and the mixtures were maintained for 24 h at RT (~22 °C). As shown in Fig. S7,† the amount of adsorbed toxin increased as the amount of added particles increased for both pC and IS as was expected. However, the uptake capacity (expressed as μmol of toxin adsorbed per g of particles) reached its maximum value for 10 mg, and therefore, this amount of particles was selected as the optimal one. Next, we studied the influence of the temperature on the removal efficiency of nanoZIF8@PMA particles by performing the adsorption experiments at RT or at 37 °C to mimic the human body temperature. As expected, the adsorption of both toxins on the nanoZIF8@PMA increased (1.4-fold and 1.5-fold for pC and IS, respectively) with the increase of temperature because the higher temperature facilitated diffusion (Fig. 1E). After that, kinetic studies were performed at 37 °C by varying the incubation time of the adsorption experiments (Fig. 1F). The results revealed the rapid adsorption of toxins in the first minutes of incubation, reaching removal efficiencies of 69% and 55% for pC and IS respectively, in just 1 h. In particular, the adsorption rate of pC from 1 h to 3 h was faster (a greater slope of the kinetic curve) than for IS, suggesting a stronger interaction between pC and nanoZIF8@PMA compared with IS. The faster diffusion of pC molecules can be understood by considering its smaller size, which would allow its easier passage through ZIF-8 windows (Fig. 1G). Under optimized conditions (10 mg of nanoZIF8@PMA, 5 mL of 0.3 mM pC or IS solutions in PBS pH = 7.4, and an incubation time of 3 h at 37 °C), the removal efficiencies reached 87.5 ± 3.2% for pC and 66.0 ± 2.8% for IS. The fact that nanoZIF8@PMA particles exhibited higher adsorption capacity as well as faster adsorption kinetics for pC than for IS is not surprising due to the following reasons: (i) the pores of ZIF-8 are highly hydrophobic, and therefore hydrophobic molecules such as pC will be more likely adsorbed; (ii) IS is a bulkier molecule, and consequently more difficult to diffuse through the porous structure of ZIF-8. It is also worth noting that although both pC and IS molecules are slightly larger than the theoretical limiting window size of ZIF-8 (3.4 Å, as estimated from the XRD data), it is known that molecules larger than this size can diffuse through ZIF-8 thanks to the flexibility of the framework.

In order to better understand the adsorption behaviour of both toxins in ZIF-8, we carried out Grand Canonical Monte Carlo (GCMC) simulations. These simulations showed that the two molecules are readily adsorbed within the ZIF-8 pores (Fig. 1H). Although the theoretical maximum loadings for both toxins are higher than the experimental ones (see the ESI† for details), they are in agreement with the experimental observation that pC has a higher loading than IS. The difference between the theoretical and experimental values of toxin loadings is likely due to the difference between the simulated model (i.e., considering the adsorption of a phase of pure

molecules) and the real solutions (i.e., toxins are in a PBS solution). Indeed, additional simulations by increasing the complexity of the model, specifically including sodium phosphate species, revealed that the theoretical adsorption loadings of toxin molecules decreased significantly due to the competition with sodium phosphate (Fig. S17†). In any case, the satisfactory adsorption values found experimentally, and supported theoretically, for both toxins (pC and IS) indicated the promising potential of nanoZIF8@PMA particles to remove these toxins.

Next, the effect of the adsorption of the toxins on the crystallinity of the particles was investigated by PXRD, revealing that the crystalline structure of nanoZIF8@PMA was completely preserved (Fig. S8†), which is a key aspect in view of a potential reuse of the particles. Comparing our values with those reported for other MOFs under static conditions,[11,13] specifically for pC or its sulfate derivative (pCS) toxin, it can be concluded that the adsorption capacity of nanoZIF8@PMA synthesized in this work is of the same order as the best values reported by Kato et al. for NU-1000 and NU-901 (Fig. 1G and Table S3†).

To investigate whether nanoZIF8@PMA could be retained within a decellularized kidney scaffold, we carried out experiments with fluorescent-labelled nanoZIF8@PMA particles to easily monitor the immobilization and potential leaking. To this end, a bright red-fluorescent dye, specifically rhodamine B (RhB), was loaded during the synthesis of the ZIF-8 particles (before PMA modification) to maximize the amount of dye incorporated into the nanostructure (loading percentage 73%); see the ESI† for preparation of RhB-nanoZIF8 and RhB-nanoZIF8@PMA particles. We used an acellular renal scaffold because it is a better representation of the natural kidney environment compared to other synthetic polymer scaffolds, as the extracellular matrix maintains the 3D ultrastructure and the physico–chemical properties of the native kidney. The scaffold was prepared by performing an optimized decellularization process, as reported previously (see the ESI†).[21] After the decellularization process, the kidney became translucent due to the removal of the cellular component (Fig. 2B; compared with the native kidney in Fig. 2A). Moreover, histologic evaluation with hematoxylin and eosin (H&E) staining confirmed the absence of cellular content and the preservation of the renal microarchitecture. The fluorescent RhB-nanoZIF8@PMA particles were further introduced into the scaffold by manual perfusion through the renal artery (Fig. S9†), followed by perfusion with PBS (washing step) the next day to remove unretained nanoparticles. The amount of nanoZIF8@PMA perfused was optimized to achieve a quantitative immobilization within the scaffold (i.e., 8.3 mg of nanoZIF8@PMA per gram of scaffold; see the ESI†). It should be noted that the control of the quantity of nanoparticles immobilized is essential to subsequently achieve batch-to-batch reproducibility. Confocal microscopy images of transverse sections of the kidney scaffold revealed the successful retention of the nanoZIF8@PMA particles in the scaffold; they were localized within the extracellular matrix, mainly in the
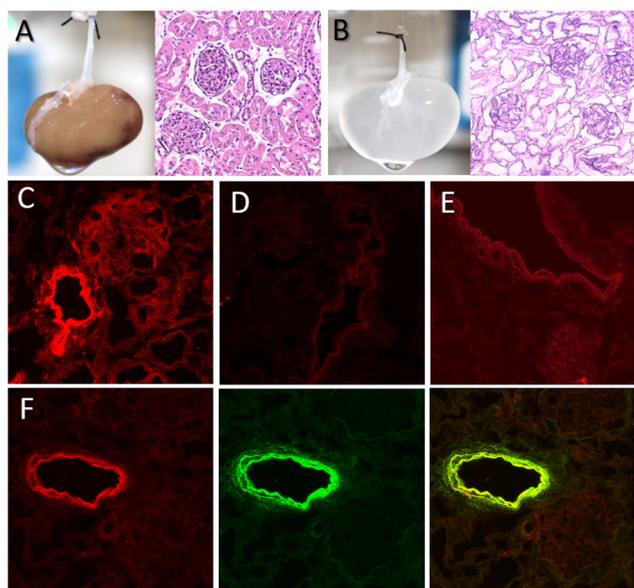
Fig. 2 Photograph of (A) a native kidney scaffold and (B) a decellularized scaffold, both with their corresponding H&E staining. (C–F) Representative confocal microscopy images (40× magnification) of scaffolds after perfusion of (C) RhB-nanoZIF8@PMA particles, (D) RhB solution, (E) RhB-nanoZIF8 particles without the PMA coating, and (F) doubly fluorescent-labelled RhB-nanoZIF8@PMA-FA particles, showing the red fluorescence channel for RhB (λ_{ex} = 514 nm, λ_{em} = 575–650 nm), a green channel for FA (λ_{ex} = 488 nm, λ_{em} = 500–575 nm), and a merge image.

vascular network (Fig. 2C), as shown in the images using fluorescent RhB-nanoZIF8@PMA particles to monitor the retention. Control experiments with the free fluorescent dye showed negligible fluorescence within the scaffold (Fig. 2D), indicating that the free dye was not strongly retained, and it was thus eliminated during the washing step. To gain further insight into the role of PMA on the retention of the nanoparticles in the scaffold, fluorescent RhB-nanoZIF8 particles (without PMA coating) were perfused through a scaffold under identical conditions. Qualitative results from the confocal microscopy images (Fig. 2E) indicated a much lower retention compared to RhB-nanoZIF8@PMA particles, which is more likely due to the degradation of the nanoZIF8 particles during the immobilization process (perfusion and washing step with PBS), with the consequent release of the fluorescent RhB molecules previously loaded into the particles, followed by their removal out of the scaffold. This may be logical considering that we have already seen that nanoZIF8 particles are not stable in PBS, as confirmed by PXRD.

To further assess the structural stability of the nanoZIF8@PMA particles during the immobilization, we performed additional experiments with doubly fluorescent-labelled nanoparticles, specifically, RhB-nanoZIF8@PMA-FA particles, where PMA modified with fluoresceinamine (FA) was used for coating the RhB-nanoZIF8 particles. After the perfusion of RhB-nanoZIF8@PMA-FA through the scaffold, the typical green fluorescence of FA was not observed in the

washing solutions, which allowed us to rule out a possible detachment of PMA from nanoZIF8 particles during or after retention. Moreover, confocal microscopy showed a high degree of colocalization of both fluorescent channels, that is, core particles labelled with red RhB and the polymer coating labelled with green FA (Fig. 2F and Fig. S10†), revealing that the nanoZIF@8PMA particles maintained their structural integrity once immobilized within the renal scaffold. All these experiments clearly pointed out that the PMA functionalization of nanoZIF8 is critical not only to provide stability under physiological conditions (*i.e.* PBS exposure), but also to achieve successful retention on the scaffold and stability once immobilized.

With this nanoZIF8@PMA-modified scaffold at hand (in the following referred to as the ZIF8-scaffold), we sought to explore whether the nanoZIF8@PMA particles preserve their sorption properties once immobilized. For this, ZIF8-modified scaffolds were perfused with pC or IS solutions (0.3 mM in PBS) under physiological flow conditions (12 mL h^{-1} flow rate) using a closed system bioreactor (Fig. 3A and B). Note that we tried to simulate real conditions of one specific current dialy-
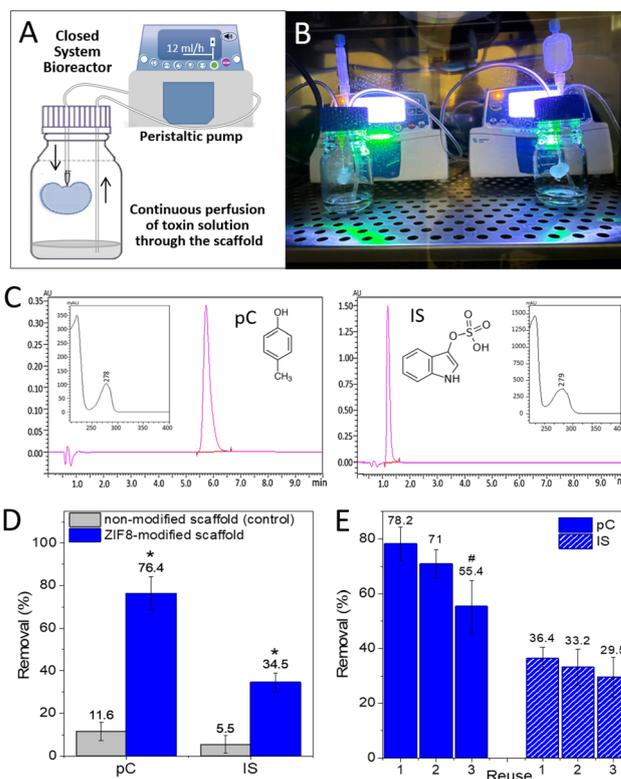

Fig. 3 Scheme (A) and photograph (B) of a closed loop perfusion bioreactor. (C) Representative RP-HPLC-DAD chromatograms for pC and IS; insets show the UV-Vis spectrum of each toxin. (D) Removal efficiencies of the ZIF8-scaffold compared to the control scaffold; conditions: 10 mL of 0.3 mM pC or IS solution in PBS (or the human serum) passing through the scaffold for 24 h at 12 mL h^{-1} flow rate. The results are shown as means ± SD of three independent experiments. *p < 0.001 *vs.* non-modified scaffold. (E) Reusability of the ZIF8-scaffold. Data are expressed as mean value ± SD of three independent experiments. #p < 0.05 *vs.* reuse 1.

sis technique, in particular hemodiafiltration with the regeneration of the ultrafiltrate by adsorption. To quantify the adsorption efficiency of the ZIF8-scaffold, the concentrations of toxins in the solutions collected after continuous perfusion for 24 h were determined using an analytical reversed phase-high performance liquid chromatography-diode array detector (RP-HPLC-DAD; Fig. 3C and S11; see the ESI† for details). Gratifyingly, we observed a significant decrease in the concentration of toxins passing through the ZIF8-scaffold as depicted in Fig. 3D. Removal efficiencies of 76% and 34% for pC and IS, respectively, were achieved after 24 h of perfusion. Control experiments using non-modified scaffolds confirmed the need for the nanoZIF8@PMA particles to promote the adsorption of toxins (Fig. 3D). It is important to note that the experiments were rather reproducible (with standard deviations of <10% working with different scaffolds). As expected, the removal efficiency was higher for pC than for IS, which is in agreement with the above discussed results under static conditions.

Going a step further, we wanted to test whether our ZIF8-scaffold could be used for removing uremic toxins directly from the human serum instead of using a solution of toxins in PBS (mimicking the ultrafiltrate in the adsorption-based dialysis method of hemodiafiltration). For this, commercially available human serum was fortified with both toxins (at 0.3 mM each) and perfused through the ZIF8-scaffold following the same procedure as previously described. The results showed that the removal efficiency for IS was identical to that obtained in PBS (34%), while for pC it was only slightly lower (69%), Fig. S12.† Note that we had to change the HPLC-DAD method to properly analyse (separate and quantify) both toxins in the presence of interferences from the serum (see the ESI†).

Moreover, to evaluate the real potential of our approach, we examined the feasibility of reusing the ZIF8-scaffold, which can be especially relevant in terms of accomplishing the long-term goal of developing "functional artificial kidneys". For that, the ZIF8-scaffold was used to remove pC from a solution (0.3 mM pC in PBS) that passes through it (reuse 1), as previously described, and the removal efficiency was quantified by RP-HPLC-DAD. Then, the ZIF8-scaffold was washed by manual perfusion with PBS to remove toxins weakly adsorbed on the scaffold, and a fresh pC solution was again perfunded for an additional 24 h (reuse 2). This cycle was repeated one more time (reuse 3). Fig. 3E shows the removal efficiency after each use, demonstrating that although the adsorption efficiency decreased considerably in the third use, the ZIF8-scaffold was still effective. Additionally, no zinc could be detected by ICP-OES in the perfused solution after the third reuse confirming that the nanoZIF8@PMA particles did not decompose even after several cycles of perfusion under flow conditions. The decrease in the adsorption capacity of the ZIF8-scaffold after several uses can be attributed to the reduction of free pores available in the MOF structure (reaching almost a saturation condition) and/or partial blocking of the outer pores and channels by molecules previously adsorbed on the surface. Unfortunately, we failed in several attempts to regenerate the ZIF8-scaffold. Mild treatments did not remove the strongly

adsorbed toxins from the ZIF8-scaffold, while strong treatments caused the nanoparticles to leak out of the scaffold. Currently, this is the main limitation of our approach, but we are working to overcome this problem.

Finally, in order to check whether the particles remained at the same locations within the renal scaffold after reuses, we did the same reusability experiment but using a scaffold modified with fluorescent-labelled nanoZIF8@PMA particles. Comparing the confocal images of the ZIF8-scaffold before and after three uses (Fig. S13†), it is clearly seen that the particles are still located at the vascular structures even after many hours of continuous perfusion of solutions, confirming their strong interaction with the vascular networks within the decellularized kidney scaffold.

Conclusions

Altogether, the main findings of this work can be summarized as follows: (i) nanoZIF8@PMA particles could be successfully immobilized on the ECM of an acellular kidney scaffold, and importantly, they were retained even under flow conditions, which mimics the real dynamic working conditions of kidneys; (ii) the polymer coating on the nanoZIF8 particles plays a critical role in conferring stability in the scaffold microenvironment and also favours the strong interaction with the ECM; and (iii) nanoZIF8@PMA particles retained their adsorption capacity for removing toxins, mainly hydrophobic p-cresol, under such flow conditions and in a recurrent manner (up to 3 reuses with an efficiency decrease <30%).

This work represents a pioneering demonstration of functional MOF-modified scaffolds and may set the basis for the development of "artificial organs". However, to achieve such an ambitious goal, further work will be needed to expand the scope of MOF-modified kidney scaffolds to remove a broader range of uremic toxins, including protein-bound toxins. To this end, we plan to immobilize different MOFs within the same scaffold to simultaneously exploit the different adsorption properties depending on the MOF type, as well as to design MOFs with hierarchical porosity (involving micro and mesopores) to broaden the size range of toxins that can be filtered.

Experimental

The details on materials and methods can be found in the ESI.†

Author contributions

C. C.-C. conceived the idea. C. C.-C. and F. G. designed the research. C. C.-C. synthesized and characterized the materials. F. G. and V. P. performed the experiments with kidney scaffolds. S. H. carried out the computational studies. C. C.-C. and F. G. carried out formal analysis and data

curation. A. M.-M. and P. A. were involved in planning and supervising the work. All authors contributed to the results, discussion, and manuscript writing.

Conflicts of interest

There are no conflicts to declare.

Acknowledgements

References

1 National Institute of Diabetes and Digestive and Kidney Diseases, Kidney Diseases Statics for the United States, **https://www.niddk.nih.gov/health-information/health-statistics/kidney-disease**, accessed: December, 2021.

2 A. K. Bello, M. Alrukhaimi, G. E. Ashuntantang, S. Basnet, R. C. Rotter, W. G. Douthat, R. Kazancioglu, A. Köttgen, M. Nangaku, N. R. Powe, S. L. White, D. C. Wheeler and O. Moe, *Kidney Int. Suppl.*, 2017, **7**, 122.

3 R. Vanholder, R. De Smet, G. Glorieux, A. Argilés, U. Baurmeister, P. Brunet, W. Clark, G. Cohen, P. P. De Deyn, R. Deppisch, B. Descamps-Latscha, T. Henle, A. Jörres, H. D. Lemke, Z. A. Massy, J. Passlick-Deetjen, M. Rodriguez, B. Stegmayr, P. Stenvinkel, C. Tetta, C. Wanner and W. Zidek, *Kidney Int.*, 2003, **63**, 1934.

4 S. Magnani and M. Atti, *Toxins*, 2021, **13**, 246.

5 P. Molina, J. Peiró, M. A. Martínez-Gómez, B. Vizcaíno, C. Esteller, M. González-Moya, M. García-Valdelvira, M. D. Molina and F. Maduell, *Kidney Dial.*, 2021, **1**, 121.

6 P. Ciceri and M. Cozzolino, *Toxins*, 2021, **13**, 380.

7 V. Wernert, O. Schäf, H. Ghobarkar and R. Denoyel, *Microporous Mesoporous Mater.*, 2005, **83**, 101.

8 B. Koubaissy, J. Toufaily, Z. Yaseen, T. J. Daou, S. Jradi and T. Hamieh, *Adsorpt. Sci. Technol.*, 2017, **35**, 3.

9 M. Sternkopf, S. Thoröe-Boveleth, T. Beck, K. Oleschko, A. Erlenkötter, U. Tschulena, S. Steppan, T. Speer, C. Goettsch, V. Jankowski, J. Jankowski and H. Noels, *Toxins*, 2019, **11**, 389.

10 C. X. Yang, C. Liu, Y. M. Cao and X. P. Yan, *RSC Adv.*, 2014, **4**, 40824.

11 S. Kato, K. Otake, H. Chen, I. Akpinar, C. T. Buru, T. Islamoglu, R. Q. Snurr and O. K. Farha, *J. Am. Chem. Soc.*, 2019, **141**, 2568.

12 S. Kato, R. J. Drout and O. K. Farha, *Cell Rep. Phys. Sci.*, 2020, **1**, 100006.

13 H. Cuchiaro, J. Thai, N. Schaffner, R. R. Tuttle and M. Reynolds, *ACS Appl. Mater. Interfaces*, 2020, **12**, 22572.

14 K. Dymek, G. Kurowski, L. Kuterasiński, R. Jędrzejczyk, M. Szumera, M. Sitarz, A. Pajdak, L. Kurach, A. Boguszewska-Czubara and P. J. Jodłowski, *ACS Appl. Mater. Interfaces*, 2021, **13**, 45149.

15 H. Furukawa, K. E. Cordova, M. O'Keeffe and O. M. Yaghi, *Science*, 2013, **341**, 1230444.

16 L. D. Chaves, S. Abyad, A. M. Honan, M. A. Bryniarski, D. I. McSkimming, C. M. Stahura, S. C. Wells, D. M. Ruszaj, M. E. Morris, R. J. Quigg and R. Yacoub, *JCI Insight*, 2021, **6**, 144410.

17 J. Z. Zhu, J. Zhang, K. Yang, R. Du, Y. J. Jing, L. Lu and R. Y. Zhang, *Nephrol., Dial., Transplant.*, 2012, **27**, 4323.

18 M. J. Velásquez-Hernández, R. Ricco, F. Carraro, F. T. Limpoco, M. Linares-Moreau, E. Leitner, H. Wiltsche, J. Rattenberger, H. Schröttner, P. Frühwirt, E. M. Stadler, G. Gescheidt, H. Amenitsch, C. J. Doonan and P. Falcaro, *CrystEngComm*, 2019, **21**, 4538.

19 C. Carrillo-Carrión, R. Martínez, M. F. Navarro Poupard, B. Pelaz, E. Polo, A. Arenas-Vivo, A. Olgiati, P. Taboada, M. G. Soliman, U. Catalán, S. Fernández-Castillejo, R. Solà, W. J. Parak, P. Horcajada, R. A. Alvarez-Puebla and P. del Pino, *Angew. Chem.*, 2019, **131**, 7152.

20 R. Martínez, C. Carrillo-Carrión, P. Destito, A. Alvarez, M. Tomás-Gamasa, B. Pelaz, F. Lopez, J. L. Mascareñas and P. del Pino, *Cell Rep. Phys. Sci.*, 2020, **1**, 100076.

21 F. Guerrero, A. Carmona, R. Ortega, S. Cañadillas, R. Crespo, C. Herrera and P. Aljama, *JBiSE*, 2017, **10**, 509.